Atomistic Simulations of Dislocations in Confined Volumes

P.M. Derlet, P. Gumbsch, R. Hoagland, J. Li, D.L. McDowell, H. Van Swygenhoven, and J. Wang

Abstract

Internal microstructural length scales play a fundamental role in the strength and ductility of a material. Grain boundaries in nanocrystalline structures and heterointerfaces in nanolaminates can restrict dislocation propagation and also act as a source for new dislocations, thereby affecting the detailed dynamics of dislocation-mediated plasticity. Atomistic simulation has played an important and complementary role to experiment in elucidating the nature of the dislocation/interface interaction, demonstrating a diversity of atomic-scale processes covering dislocation nucleation, propagation, absorption, and transmission at interfaces. This article reviews some atomistic simulation work that has made progress in this field and discusses possible strategies in overcoming the inherent time scale challenge of finite temperature molecular dynamics.

Introduction

Interface- or grain boundary (GB)-dominated materials can exhibit extraordinary mechanical properties in terms of yield stress and ductility, particularly when the length scale associated with the interfaces approaches the sub-100 nanometer regime.[1,2] Well-known examples are metallic nanocrystalline materials, which demonstrate significant increases in yield stress when the mean grain size falls below 100 nm.[1–4] Particularly strong, but still deformable, microstructures also can be achieved in materials of low stacking fault energy by introducing a high density of nanoscale twins into an otherwise coarser microstructure.[5,6]

The mechanical response of coarse-grained polycrystals has been modeled by mesoscopic techniques such as the 3D dislocation dynamics simulation method.[7–9] In these methods, traditional ideas of dislocation nucleation/multiplication via Frank-Read like dipole sources are used, in which the fundamental mechanism is the dislocation-dislocation interaction. In this regime, GBs primarily enforce plastic macroscopic compatibility, but as the grain size is reduced, the role of the GB as both a dislocation source and barrier must be taken explicitly into account. Representing GBs as impenetrable barriers within the framework of 2D dislocation dynamics has constituted one strategy that begins to address these issues.[10,11] The GB dislocation nucleation aspect also has been included in larger length-scale modeling methods.[12–14] Such approaches all assume empirical laws whose origins are fundamentally atomistic, and it is from this perspective that molecular dynamics (MD) simulation can play an important role in the study of plasticity, since it allows for a detailed investigation of the underlying atomic scale processes that lead to dislocation nucleation, absorption, and transmission at a GB.

In this article, the various aspects of the dislocation–interface interaction studied by atomistic simulation methods are reviewed, and a number of concrete examples are given spanning dislocation nucleation, propagation, absorption, and transmission at an interface. Possible strategies are discussed to go beyond the high strain rate regime of classical MD through the use of reaction pathway and activation volume calculations.

Dislocation Nucleation

To investigate dislocation nucleation at a GB by atomistic simulation, a simple dislocation bicrystal atomic configuration geometry often is used: an atomic configuration consisting of two differently orientated crystal lattices, one existing in the upper half of the simulation cell and the other existing in the lower half. This allows for a systematic study of the dislocation nucleation process as a function of both loading and misorientation between the two crystals and is ideally suited to the study of high-angle coincident site lattices (CSL), a class of GBs in which the neighboring crystal lattices contain a subset of coincident lattice sites. The ratio of the corresponding CSL primitive cell to the crystal lattice primitive cell defines the Σ number of the GB and is always an integer. Such boundaries can play an important role in the properties of polycrystalline materials, particularly in heterolayer structures and nanocrystalline metals, where through GB engineering the fraction of these GBs can be increased.[16]

A GB may be described in terms of an array of dislocations of differing Burgers vector directions and magnitudes that together accommodate the associated misorientation of the neighboring lattices. The Burgers vector content of a GB can either increase or decrease following a dislocation nucleation event and can be rationalized as a reaction that conserves the total Burgers vector content of the system (lattice plus interface dislocation content). The CSL $\Sigma 3$ asymmetric tilt GB in Cu of intermediate inclination angle[15] shown in Figure 1a has a partial dislocation (see black arrow in the upper part of Figure 1a) that is dissociated from the boundary on the maximum Schmid factor plane (highest resolved shear stress); this is the same (111) plane onto which the dislocation is emitted into the adjoining lattice upon tensile loading normal to the interface. In this case, the emission of the partial dislocation reduces the Burgers vector content of the GB since the total Burgers vector content of the system must be conserved. For a $\Sigma 3$ asymmetric tilt GB of low inclination angle,[15] the Burgers vector content increases following dislocation nucleation. In this case, a GB dislocation is initially dissociated from the boundary on a $\langle 111 \rangle$ slip plane of low resolved shear stress (Schmid factor = 0.148), as shown in Figure 1b top left for Cu.

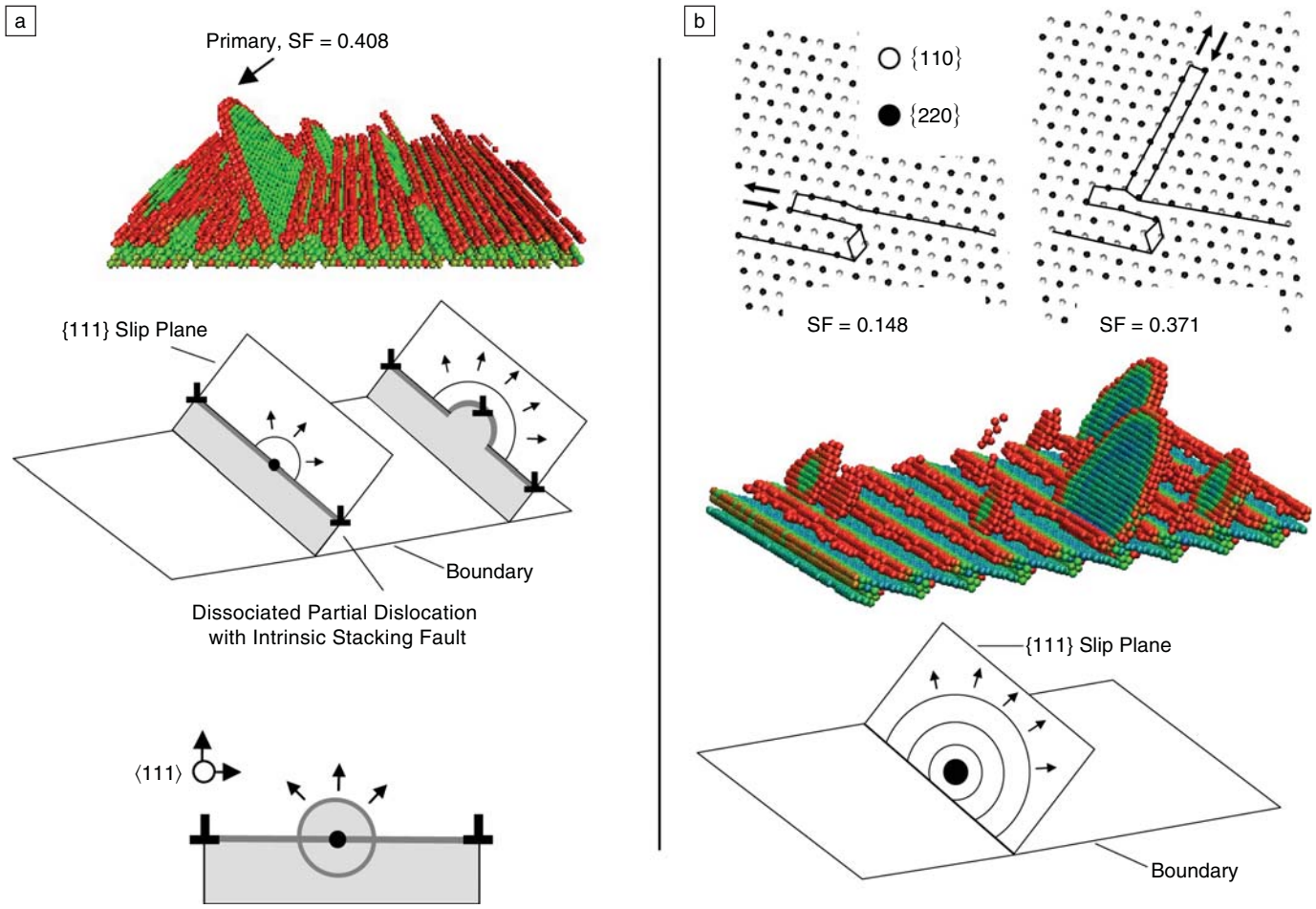

Figure 1. (a) Example of dislocation nucleation for a Σ3 asymmetric tilt grain boundary of intermediate inclination angle, with nucleation on the same (111) plane as the initial dissociation. (b) For a low inclination angle, Σ3 asymmetric tilt grain boundary, dislocation loops nucleate homogeneously in the lattice at a dislocation source near the intersection of two boundary facets on the maximum Schmid factor (SF) plane.[15]

Figure 1b top right shows that upon application of tensile stress normal to the interface, a partial dislocation loop nucleates on a {111} slip plane of high-resolved shear stress (Schmid factor = 0.371) very near the facet intersection (or GB ledge), as shown in Figure 1b middle. The GB Burgers vector content is increased since half of the dislocation loop is absorbed by the boundary, while the other half of the loop glides into the lattice. From a parametric study of symmetric and asymmetric tilt GBs in Cu and Al,[16–24] it became clear that the stress magnitudes required to nucleate dislocations are somewhat less than those for homogeneous nucleation of dislocations in single crystals.[18,24] Moreover, nucleation of partial dislocations from the interface upon application of a tensile stress normal to the boundary is generally of non-Schmid character (i.e., a slip plane that is not geometrically predicted), indicating the important role local GB structure can play in the nucleation process.

An inherent restriction of the simple bicrystal geometry is the 2D planar nature of the GBs and the restricted class of misorientations that can be studied. Moreover, the effect of triple and quadruple junctions cannot be studied. To study these features, a fully 3D GB network must be considered. Computer-generated 3D nanocrystalline samples can be constructed geometrically using the Voronoi procedure, which partitions the simulation cell volume into polyhedra, each of which has a crystal lattice orientation assigned to it, resulting in planar GBs with interface structures that are well ordered in terms of misfit and coherent regions.[25–31] For the face-centered-cubic (fcc) grains, random orientations are generally chosen, producing a wide variety of general GBs and boundaries close to coincident lattice site misorientations.[28] A central result of atomistic nanocrystalline simulation has been that local GB structures can strongly affect where dislocations are nucleated: misfit regions. Ledge structures or triple junction lines containing large local stresses can act as nucleation sites for partial dislocations (see Figure 2a). Via atomic shuffling and/or free-volume migration either before or after nucleation, such regions also undergo structural relaxation.[31,32] Often these anomalous stresses evolve during deformation due to a local sliding incompatibility,[29] demonstrating the close relationship between GB accommodation processes and slip activity within the nanocrystalline environment. Such an interplay between dislocation nucleation at GBs and GB sliding also has been studied in bicrystal geometries (see References 33 and 34).

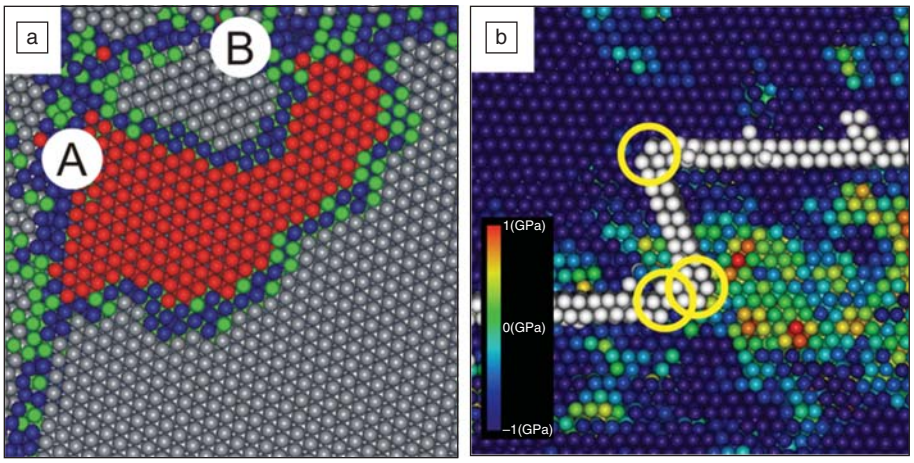

Figure 2. (a) Snapshot of a nucleated dislocation segment where (A) and (B) represent the grain boundary (GB) regions in which the leading partial and trailing partial dislocations are respectively nucleated. Atoms are colored according to the common-neighbor analysis method, where grey represents fcc atoms, red hcp atoms, blue non-12-coordinated atoms, and green 12-coordinated atoms without an identifiable symmetry. The blue and green atoms identify the GB region. (b) Picture of a dislocation that has cross-slipped (see circles) within a grain, where the white atoms represent atoms neighboring the slip plane of the dislocation. The GB atoms are colored according to their local hydrostatic pressure, where atoms under tension greater than –1 GPa are colored blue, and those under compression greater than 1 GPa are colored red. For intermediate coloring, see the linear color bar.

Dislocation Propagation and Absorption

In the 3D geometry of a nanocrystalline network, the structure of the nearby GBs and triple junctions can strongly affect the behavior of the expanding dislocation loop. For example, the anomalous stress intensities at misfit regions can, in addition to acting as nucleation sites, also hinder propagation, pinning the dislocation for a time that depends on both the local shear stress and temperature.[35] Propagation between pinning/de-pinning events is mechanically driven and therefore not strongly temperature dependent. More recent work has shown that propagating dislocations can avoid such pinning sites by cross-slipping via the Fleischer mechanism[36] to another slip-system. In the Fleischer mechanism, the leading partial dislocation first changes its glide plane by the creation of a stair rod dislocation with which the trailing partial reacts to also change its glide plane, thus choosing a more favorable path in which to deposit the Burgers vector content in the surrounding GB network[37] (see Figure 2b). Atomistic simulation therefore suggests a complex picture for nanoscale plasticity in which GB structure plays a critical role in determining the nature of local slip. Recent constant strain rate tensile simulation work indicates that as the global stress increases from zero, nonpropagating dislocation segments nucleate at the GB.[31] These pinned dislocation segments are observed to propagate only when the resolved shear stress reaches a critical value that depends sensitively on the local environment, a result that points to propagation being the rate-limiting process in such high strain rate simulations. By following the average resolved shear stresses within a grain, it was found that rapid drops could be correlated with slip activity in that grain. By recording the shear stress on a slip system just before such dislocation activity occurs, a distribution of so-called critical shear stresses is obtained; it is found, for the strain rate studied, to center on that predicted by the Sachs model[38], which is derived from an orientational average of the maximum shear stress of an isotropic distribution of grain orientations. Such a distribution of critical shears appears to be necessary for constitutive models to produce nanocrystalline stress-strain curves similar to those seen in experiments—with an extended micro-plastic regime before the onset of true macroscopic plasticity.[12,14]

Bicrystal geometries also have been employed in the atomistic study of dislocation absorption at interfaces, in particular, to study the mechanical properties of metallic nanolayered composites. Such materials have two or more different metals alternating many times[39,40] and exhibit high strength due to the difficulty of slip transfer across the interfaces.[41–49] Well-studied systems are the CuNb-based composites, where a bilayer system consisting of Cu and Nb crystals adopts the Kurdjumov-Sachs (KS) crystallographic orientation relation[39,40,45,50]—a commonly observed orientation relation between close-packed planes of neighboring fcc and body-centered-cubic (bcc) solids. Atomistic simulations have revealed that atomic structures of Cu/Nb interfaces can have multiple states with nearly degenerate energies,[41,42,44,47–49], such as the KS_1 atomic structure formed by directly combining two semi-infinite perfect crystals according to the KS orientation relation,[42,44,47] and two other types of atomic structures, KS_2 and KS_{min}, formed by inserting an intermediate Cu monolayer into the KS_1 interface.[41,42,48,49]

Because the shear resistance of Cu/Nb interfaces is low, non-uniform, and strongly anisotropic, dislocation core spreading is expected to be complex in the interface when a lattice dislocation enters and also dependent on the type of KS structure. Through atomistic simulations, it has been shown that a leading Shockley partial dislocation, no matter what type or sign, enters the interface[42,48] and readily spreads into intricate patterns, as shown in Figure 3. The spatial variation of interface shear resistance determines these patterns. Within the KS_1 interface, the core width is about 4 nm, which is more than 15 times the value of the Burgers vector for a Shockley partial dislocation in Cu. Similar features are observed for the interaction of lattice dislocations with the interfaces in the Nb crystal.[41,48,51] As a consequence, it is extremely difficult for a glide dislocation to compact in the interface plane so that it can be emitted into adjacent layers. Such a "trapping" of dislocations is somewhat more effective in KS_2 than KS_1 because the interfacial shear resistance is lower for KS_2.[42]

Slip Transmission

Under bicrystal geometries, atomistic simulation has allowed the systematic study of slip transmission as a function of GB type and stress state. For example, a common theme has been a GB's resistance to intergranular dislocation slip transmission. Early atomistic work[52] introduced dislocations via an artificial crack tip and found that dislocation transmission depended on three parameters: (1) the ratio of the incoming and outgoing resolved shear stresses, (2) the magnitude of the residual Burgers vector, and (3) the angle between the incoming and outgoing

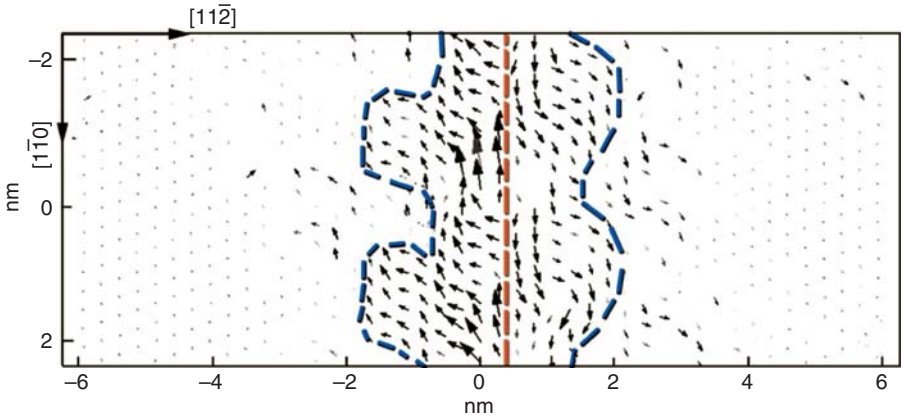

Figure 3. Patterns in the vector field plot disregistry (in nm) across the interface plane, showing core spreading for an edge Shockley partial entering KS_1 interface from the Cu crystal. The viewing direction is parallel to the interface normal. The orange dashed line indicates the intersection of the slip plane with the interface. The blue dashed lines are interfacial dislocations separating the slipped regions from the nonslipped regions.

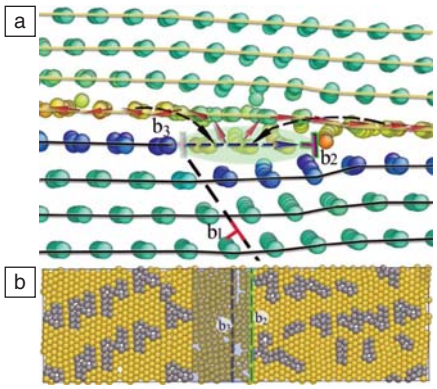

Figure 4. CuNb atomic structures after the dislocation labeled b_1 enters the interface from the Nb crystal. In (a) the dislocation dissociates into an interfacial dislocation labeled b_2 and interfacial discontinuity labeled b_3 via Cu atom migration within the interface. The red arrows indicate the diffusion of vacancies, and the black arrows represent the counter diffusion of Cu atoms. (b) A view (parallel to the interface normal) of the atomic structure of the interfacial Cu plane where the regions with low areal density of Cu atoms are outlined in grey atoms and the grey shadow.

slip plane intersections with the GB. GB structure also can play a critical role in local slip transmission. Atomistic simulation has shown that if the angle between intersecting slip plane is small, regions of lattice continuity across a general high-angle GB can facilitate dislocation activity in the neighboring grain.[53]

The dislocation transmission properties of symmetric CSL Σ3 boundaries (i.e., coherent twin boundaries [TBs]) play a critical role in the strongly anisotropic response of fcc materials whose microstructure is characterized by a high-density stacking of twin lamellae.[5,54] For general plastic deformation, shearing of the twins must be considered, and two different types of dislocation/TB interaction are possible: (1) shearing of the TB in a direction contained within the TB may be achieved by depositing perfect screw dislocations at the TBs;[55,56] (2) any macroscopic direction of shear that intersects the TB may be achieved by the interaction of non-screw dislocations with the TBs that can lead to slip transmission.[56]

To investigate the relevant pathways by which slip may be transmitted through TBs, quasi 2D atomistic simulations have been used.[55] The main result of these simulations is that the expected outcome, a straight transmission of the incoming dislocation into the twinned crystal with the generation of a local defect in the TB, is by far not the only process and not the most likely process either. For example, the incoming dislocation can nucleate a twinning partial in the TB, thereby changing its own character into a sessile lock, an immobile dislocation structure. Such sessile defects are also created if only partial dislocations can leave the TB. Depending on the loading situation, this is what is generally observed in Al and sometimes in Ni and Cu. For the case of screw dislocations, it is important to realize that the perfect screw dislocation may penetrate the TB, but the partial dislocations, which it is composed of, have to change their order during passage. As a consequence, the screw dislocation first has to form a constriction at the TB before it can be re-emitted into the neighboring grain.[55] Moreover, the screw dislocation will not always be re-emitted but instead may be incorporated into the TB as two twinning partials. The competing processes of generating the twinning partials or generating the partials of the lattice dislocation can be reasonably well reconciled with the relative cost of generating the corresponding unstable defects.[55] More detailed analysis will require the competing processes to be treated in a fully 3D activation analysis.

It is generally believed that dislocation transmission across interfaces can be enabled if motion of GB dislocations is easy within the interface. For the case of the nanolayered composite materials, atomistic simulations reveal that the low shear resistance of Cu/Nb interface enables the in-plane component of dislocations to glide with a high mobility. In addition, the out-of-plane component of dislocations can climb in the interface through absorption and emission of vacancies, as shown in Figure 4. Consequently, a patch of extra Cu {111} forms at the end of the half plane of Nb (110). By the gliding of in-plane components and the climbing of out-plane components, dislocations scattered within the interface can reassemble into glide dislocations that emerge, under stress, into adjacent layers. The rate of climb depends on the concentration and diffusivity of vacancies. Recent atomistic simulations have shown that both quantities are far higher at the interface than in the bulk.[58]

Discussion and Concluding Remarks

The examples given in this article demonstrate the power of atomistic techniques in elucidating possible processes that contribute to subsequent bulk plasticity. However, because of the short time scales that finite temperature MD can realistically simulate, the strain rate and the corresponding stresses must be high to reduce the enthalpy barriers that characterize the atomic scale plastic processes. In this sense, the processes studied are driven predominantly by high stresses that reduce the effective enthalpy barriers to near zero values. In the experimental regime, where the strain rates are typically 10 orders of magnitude lower than in atomic simulation, such barriers are overcome primarily via thermal assistance, resulting in lower effective stresses. The temperature dependence of the dislocation pinning/de-pinning propagation

mechanism seen in nanocrystalline simulations[35] indicates some degree of thermal assistance; however, the sub-nanosecond measured residence times indicate enthalpy barriers that still may be considerably smaller than those measured experimentally.

Finite temperature MD acceleration methods have offered some hope in simulating time scales closer to the experimental regime through the development of either kinetic or potential energy biasing schemes and parallel replica techniques (in which copies of an atomic system are distributed across computing nodes to increase the statistical sampling size) that are able to more efficiently overcome the associated enthalpy barriers.[59–62] These methods have been successful predominantly in the field of diffusion but more recently have been adapted to driven systems,[63] for example, in the bicrystal study of GB coupled motion[64] where experimental time scales can now be reached in simulation.[65]

How to investigate experimentally relevant strain rate effects remains a general challenge to the atomistic modeling community. The concept of activation volume, which is fundamentally related to the strain rate sensitivity in the classic theory of plasticity,[66] may provide a useful macro-micro bridge. The activation volume Ω is defined as the derivative of the activation enthalpy Q (of the rate-controlling process) with respect to stress (σ): $\Omega \equiv -\partial Q/\partial\sigma$. If one could identify the rate-controlling process and calculate its activation energy as a function of stress, then one not only could predict the flow stress at experimentally realistic strain rates (~10^{-4}/s) and finite temperature using transition-state theory,[67] but one also could directly compare it with the experimentally measured strain rate sensitivity, which is a kinetic signature of the deformation mechanism.[67,68] Experimentally measured activation volumes are typically of the order of a few to a few tens of b^3 (where **b** is the length of the full Burgers vector) for room temperature yield of heavily twinned[5] and bulk nanocrystalline[68] materials. Thus, the experimental rate-controlling saddle configurations involve just tens of atoms that are critically activated—a number that is well within the size scale accessible by atomistic calculations.

For strongly stress-driven processes, the activation enthalpy Q can be calculated by using the free-end nudged elastic band (FENEB) method,[56,68,70] a chain-of-states method for finding the minimum energy path that does not require a final stable state. FENEB has been applied to calculate the $Q(\sigma)$ of a screw dislocation absorbing into, desorbing from, and transmitting across a TB in nano-twinned copper.[56] At a local stress that gives dislocation absorption and transmission barriers in the range of 0.5–0.7 eV corresponding to experimentally easily accessible strain rates (anthropological time scales of seconds to hours), the activation volumes are calculated to be 24–44b^3. This gives a strain rate sensitivity of 0.013–0.023, a magnitude that is within a factor of two of the experimentally measured values obtained by variable rate nanoindentation (Table I). While the numerical agreement does not yet mean that these particular unit processes are the only rate-controlling processes, it does seem to confirm that dislocation/interface interactions, rather than dislocation-dislocation interactions, are the rate-controlling mechanisms in these TB-dominated materials at realistic strain rates.

In summary, atomistic simulation can play an important role in the understanding of the mechanical response of interface-dominated materials through the elucidation of the fundamental atomic scale processes that contribute to plasticity. Such processes, determined from either finite temperature molecular dynamics or transition pathway methods, cannot give directly and unequivocally the experimentally relevant rate-limiting process. However, the knowledge gained can be used either as a careful inspiration to experimental interpretation or as a basis for formulating empirical rules for use in higher-scale modeling methods.

Table I: Comparison of yield stress, activation volume, and strain-rate sensitivity between experimental measurements and atomistic calculation.

		Yield stress	Apparent activation volume Ω*	Strain-rate sensitivity m
	Uniaxial tension[6]	~1 GPa	—	—
Nano-twinned Copper	Variable-rate nanoindentation[5]	>700 MPa*	12–22b^3	0.025–0.036
	Atomistic calculation	780 MPa	24–44b^3	0.013–0.023
Diffusion-controlled processes	—	—	~0.1b^3	~1
Bulk forest hardening	—	$\sim\mu b\sqrt{\rho_{bulk}}$	100–1000b^3	0–0.005

*Extracted from the measured indentation hardness H as $\frac{H}{3}$.

Note: μ is the shear modulus, b is the full Burgers vector, and ρ_{bulk} is the bulk dislocation density.

Acknowledgments

J. Li acknowledges support by the U.S. National Science Foundation (NSF) CMMI-0728069, Office of Naval Research N00014-05-1-0504, and the Air Force Office of Scientific Research and interactions with Ting Zhu and Subra Suresh. P. Gumbsch and H. Van Swygenhoven acknowledge the financial support of the European Commission (FP6-NANOMESO, Grant No. 016710). P.M. Derlet and H. Van Swygenhoven acknowledge their work with E. Bitzek and C. Brandl and the support of the Swiss National Science Foundation. D.L. McDowell acknowledges support of the U.S. NSF and the Paden Chair in Metals Processing.

References

1. K.S. Kumar, H. Van Swygenhoven, S. Suresh, *Acta Mater*. **51**, 5743 (November 2003).
2. H. Van Swygenhoven, J.R. Weertman, *Mater. Today* **9**, 24 (May 2006).
3. H. Gleiter, *Prog. Mater. Sci*. **33**, 223 (1989).
4. M.A. Meyers, A. Mishra, D.J. Benson, *Prog. Mater. Sci*. **51**, 427 (May 2006).
5. L. Lu, R. Schwaiger, Z.W. Shan, M. Dao, K. Lu, S. Suresh, *Acta Mater*. **53**, 2169 (April 2005).
6. L. Lu, Y.F. Shen, X.H. Chen, L.H. Qian, K. Lu, *Science* **304**, 422 (April 2004).
7. B. Devincre, L.P. Kubin, *Mater. Sci. Eng. A* **8**, 234–236 (1997).
8. L.P. Kubin, G. Canova, M. Condat, B. Devincre, V. Pontikis, Y. Brchet, *Solid State Phenomena* **23–24**, 455 (1992).
9. K.W. Schwarz, *J. Appl. Phys*. **85**, 108 (1999).
10. D.S. Balint, V.S. Deshpande, A. Needleman, E. Van der Giessen, *Modell. Simul. Mater. Sci. Eng*. **14**, 409 (April 2006).
11. L. Nicola, E. Van der Giessen, A. Needleman, *Thin Solid Films* **479**, 329 (May 2005).
12. L. Li, P. M. Anderson, M-G. Lee, E. Bitzck, P. Derlet, H. Van Swygenhoven, *Acta Mater*. **57**, 8122 (2009).
13. J. Asaro, S. Suresh, *Acta Mater*. **53**, 3369 (2005).
14. D.H. Warner, J.F. Molinari, *Scripta Mater*. **54**, 1397 (April 2006).
15. M.A. Tschopp, D.L. McDowell, *Scripta Mater*. **58**, 299 (February 2008).
16. D.E. Spearot, K.I. Jacob, D.L. McDowell, *Acta Mater*. **53**, 3579 (2005).
17. D.E. Spearot, K.I. Jacob, D.L. McDowell, *Int. J. Plast* **23**, 143 (2007).

18. D.E. Spearot, M.A. Tschopp, K.I. Jacob, D.L. McDowell, *Acta Mater*. **55**, 705 (January 2007).
19. M.A. Tschopp, D.L. McDowell, *J. Mater. Sci*. **42**, 7806 (September 2007).
20. M.A. Tschopp, D.L. McDowell, *Philos. Mag*. **87**, 3147 (2007).
21. M.A. Tschopp, D.L. McDowell, *Appl. Phys. Lett*. **90**, 189901 (April 2007).
22. M.A. Tschopp, D.L. McDowell, *J. Mech. Phys. Solids* **56**, 1806 (May 2008).
23. M.A. Tschopp, D.L. McDowell, *Int. J. Plast* **24**, 191 (2008).
24. M.A. Tschopp, D.E. Spearot, D.L. McDowell, *Modell. Simul. Mater. Sci. Eng*. **15**, 693 (October 2007).
25. P.M. Derlet, A. Hasnaoui, H. Van Swygenhoven, *Scripta Mater*. **49**, 629 (October 2003).
26. P.M. Derlet, H. Van Swygenhoven, *Phys. Rev. B* **67**, 014202 (January 2003).
27. A.G. Froseth, P.M. Derlet, H. Van Swygenhoven, *Scripta Mater*. **54**, 477 (February 2006).
28. A.G. Froseth, H. Van Swygenhoven, P.M. Derlet, *Acta Mater*. **53**, 4847 (October 2005).
29. H. Van Swygenhoven, P.M. Derlet, *Phys. Rev. B* **64**, 224105 (December 2001).
30. H. Van Swygenhoven, P.M. Derlet, in *"Dislocations in Solids, A Tribute to F.R.N. Nabarro,"* J.P. Hirth, Ed. (Elsevier, 2008), vol. 14, pp. 1–41.
31. H. Van Swygenhoven, P.M. Derlet, A. Hasnaoui, *Phys. Rev. B* **66**, 024101 (July 2002).
32. P.M. Derlet, H. Van Swygenhoven, A. Hasnaoui, *Philos. Mag*. **83**, 810489 (2003).
33. B. Hyde, D. Farkas, M.J. Caturla, *Philos. Mag*. **85**, 3795 (November 2005).
34. F. Sansoz, J.F. Molinari, *Acta Mater*. **53**, 1931 (April 2005).
35. H. Van Swygenhoven, P.M. Derlet, A.G. Froseth, *Acta Mater*. **54**, 1975 (April 2006).
36. R.L. Fleischer, *Acta Metall*. **7**, 134 (1959).
37. E. Bitzek, C. Brandl, P.M. Derlet, H. Van Swygenhoven, *Phys. Rev. Lett*. **100**, 235501 (2008).
38. E. Bitzek, P.M. Derlet, P. Andersen, H. Van Swygenhoven, *Acta Mater*. **56**, 4846 (2008).
39. A. Misra, J.P. Hirth, H. Kung, *Philos. Mag. A* **82**, 2935 (November 2002).
40. A. Misra, M. Verdier, Y.C. Lu, H. Kung, T.E. Mitchell, M. Nastasi, *Scripta Mater*. **39**, 555 (August 1998).
41. M.J. Demkowicz, R.G. Hoagland, *J. Nucl. Mater*. **372**, 45 (January 2008).
42. M.J. Demkowicz, J. Wang, R.G. Hoagland, in *"Dislocations in Solids: A Tribute to F.R.N. Nabarro,"* J.P. Hirth, Ed. (Elsevier, 2008), vol. 14, pp. 141.
43. R.G. Hoagland, *J. Basic Eng*. **89**, 525 (1967).
44. R.G. Hoagland, J.P. Hirth, A. Misra, *Philos. Mag*. **86**, 3537 (August 2006).
45. R.G. Hoagland, R.J. Kurtz, C.H. Henager, *Scripta Mater*. **50**, 775 (March 2004).
46. R.G. Hoagland, T.E. Mitchell, J.P. Hirth, H. Kung, *Philos. Mag. A* **82**, 643 (March 2002).
47. A. Misra, M.J. Demkowicz, J. Wang, R.G. Hoagland, *JOM* **60**, 39 (April 2008).
48. J. Wang, R.G. Hoagland, J.P. Hirth, A. Misra, *Acta Mater*. **56**, 3109 (2008).
49. J. Wang, R.G. Hoagland, A. Misra, *J. Mater. Res*. **23**, 1009 (April 2008).
50. G.J. Wang, A.P. Sutton, V. Vitek, *Acta Metall*. **32**, 1093 (1984).
51. J. Wang, R.G. Hoagland, J.P. Hirth, A. Misra, *Acta Mater*. **56**, 5685 (2008).
52. M. de Koning, R. Miller, V.V. Bulatov, F. Abraham, *Philos. Mag. A* **82**, 2511 (2002).
53. C. Brandl, E. Bitzek, P.M. Derlet, H. Van Swygenhoven, *Appl. Phys. Lett*. **91**, 111914 (September 2007).
54. X. Zhang, A. Misra, H. Wang, M. Nastasi, J.D. Embury, T.E. Mitchell, R.G. Hoagland, and J.P. Hirth, *Appl. Phys. Lett*. **84**, 1096 (February 2004).
55. Z.H. Jin, P. Gumbsch, E. Ma, K. Albe, K. Lu, and H. Hahn, *Scripta Mater*. **54**, 1163 (March 2006).
56. T. Zhu, J. Li, A. Samanta, H.G. Kim, S. Suresh, *Proc. Nat. Acad. Sci. U.S.A*. **104**, 3031 (February 2007).
57. Z.H. Jin, P. Gumbsch, K. Albe, E. Ma, K. Lu, H. Gleiter, and H. Hahn, *Acta Mater*. **56**, 1126 (March 2008).
58. J. Wang, R.G. Hoagland, A. Misra, *Scripta Mater*. **58**, 541 (2008).
59. A.F. Voter, *Phys. Rev. Lett*. **78**, 3908 (May 1997).
60. A.F. Voter, *J. Chem. Phys*. **106**, 4665 (March 1997).
61. A.F. Voter, *Phys. Rev. B* **57**, 13985 (June 1998).
62. R.A. Miron, K.A. Fichthorn, *J. Chem. Phys*. **119**, 6210 (September 2003).
63. B.P. Uberuaga, S.J. Stuart, A.F. Voter, *Phys. Rev. B* **75**, 014301 (January 2007).
64. J.W. Cahn, Y. Mishin, A. Suzuki, *Acta Mater*. **54**, 4953 (November 2006).
65. Y. Mishin, A. Suzuki, B.P. Uberuaga, A.F. Voter, *Phys. Rev. B* **75** 224101 (June 2007).
66. U.F. Kocks, A.S. Argon, M.F. Ashby, *Prog. Mater. Sci*. **19**, 1 (1975).
67. J. Li, *MRS Bull*. **32** (6), 151 (2007).
68. T. Zhu, J. Li, A. Samanta, A. Leach, K. Gall, *Phys. Rev. Lett*. **100**, 025502 (January 2008).
69. Y.M. Wang, E. Ma, *Acta Mater*. **52**, 1699 (April 2004).
70. C. Shen, J. Li, Y.Z. Wang, *Metall. Mater. Trans. A* **39**, 976 (2008). □